PROCEEDINGS OF SCIENCE

$B \to D^{(*)} \ell \nu$ form factors from lattice QCD with relativistic heavy quarks

JLQCD Collaboration: T. Kaneko[*a,b†], Y. Aoki[c], G. Bailas[a], B. Colquhoun[d], H. Fukaya[e], S. Hashimoto[a,b] J. Koponen[a]

[a] *High Energy Accelerator Research Organization (KEK), Ibaraki 305-0801, Japan*
[b] *School of High Energy Accelerator Science, SOKENDAI (The Graduate University for Advanced Studies), Ibaraki 305-0801, Japan*
[c] *RIKEN Center for Computational Science, Kobe 650-0047, Japan*
[d] *Department of Physics and Astronomy, York University, Toronto, ON, M3J 1P3, Canada*
[e] *Department of Physics, Osaka University, Osaka 560-0043, Japan*

We report on our calculation of the $B \to D^{(*)} \ell \nu$ form factors in 2+1 flavor lattice QCD. The Möbius domain-wall action is employed for light, strange, charm and bottom quarks. At lattice cutoffs $a^{-1} \sim 2.4$, 3.6 and 4.5 GeV, we simulate bottom quark masses up to 0.7 a^{-1} to control discretization errors. The pion mass is as low as 230 MeV. We extrapolate the form factors to the continuum limit and physical quark masses, and make a comparison with recent phenomenological analyses.

37th International Symposium on Lattice Field Theory - Lattice2019
16-22 June 2019
Wuhan, China

[*]Speaker.
[†]E-mail: takashi.kaneko@kek.jp

PoS(LATTICE2019)139

1. Introduction

The $B \to D^{(*)}\ell\nu$ semileptonic decays are promising probes of new physics. However, there has been a long-standing tension in the Cabibbo-Kobayashi-Maskawa (CKM) matrix element $|V_{cb}|$ with its alternative determination from inclusive decays [1]. Phenomenological analyses [2, 3, 4, 5, 6, 7] of recent Belle data of the $B \to D^*\ell\nu$ differential decay rate [8, 9] are deepening our understanding of the systematics of the $|V_{cb}|$ determination. An unambiguous resolution of the $|V_{cb}|$ tension, however, will require a first-principle calculation of the relevant form factors by means of lattice QCD. The $B \to D^*\ell\nu$ form factors at non-zero recoils are of particular importance, and are being calculated by us and other collaborations [10, 11].

In this article, we update our results for the $B \to D^{(*)}\ell\nu$ form factors. After our previous report [12], the calculation has been extended to a larger cutoff $a^{-1} \sim 4.5$ GeV and a smaller pion mass $M_\pi \sim 230$ MeV. A notable feature of our simulations is the use of relativistic quark formulation with good chiral symmetry for all the relevant flavors. This enables us to straightforwardly study interesting B meson decays including $B \to \ell\nu$ [13] and inclusive decay [14]. Our studies of $B \to \pi\ell\nu$ [15], $B \to D^{**}\ell\nu$ [16] and $B \to K\ell\ell$ [17] are also reported in these proceedings.

2. Calculation of form factors

We generate gauge ensembles of 2+1 flavor lattice QCD at cutoffs of 2.5 – 4.5 GeV. Chiral symmetry is preserved to good accuracy by employing the Möbius domain-wall quark action [18, 19]. This simplifies the renormalization of the relevant matrix elements, which often suffers from large discretization errors. We simulate a strange quark mass m_s close to its physical value, whereas the degenerate up and down quark mass m_{ud} corresponds to pion masses as low as $M_\pi \sim 230$ MeV. The spatial lattice size L is chosen to satisfy a condition $M_\pi L \gtrsim 4$ to control finite volume effects. The statistics are 5,000 Molecular Dynamics time at each simulation point. These simulation parameters are listed in Table 1.

The $B \to D^{(*)}$ matrix elements are parametrized by six form factors in total,

$$\sqrt{M_B M_D}^{-1} \langle D(p')|V_\mu|B(p)\rangle = (v+v')_\mu h_+(w) + (v-v')_\mu h_-(w), \tag{2.1}$$

$$\sqrt{M_B M_{D^*}}^{-1} \langle D^*(\varepsilon,p')|V_\mu|B(p)\rangle = \varepsilon_{\mu\nu\rho\sigma}\,\varepsilon^{*\nu} v'^{\rho} v^{\sigma}\, h_V(w), \tag{2.2}$$

$$\sqrt{M_B M_{D^*}}^{-1} \langle D^*(\varepsilon,p')|A_\mu|B(p)\rangle = -i(w+1)\,\varepsilon^*_\mu\, h_{A_1}(w) + i(\varepsilon^* v)\, v_\mu\, h_{A_2}(w) + i(\varepsilon^* v)\, v'_\mu\, h_{A_3}(w), \tag{2.3}$$

Table 1: Simulation parameters. Quark masses are bare value in lattice units.

lattice parameters	m_{ud}	m_s	M_π[MeV]	M_K[MeV]
$\beta=4.17,\ a^{-1}=2.453(4),\ 32^3\times64\times12$	0.0190	0.0400	499(1)	618(1)
	0.0120	0.0400	399(1)	577(1)
	0.0070	0.0400	309(1)	547(1)
$\beta=4.17,\ 48^3\times96\times12$	0.0035	0.0400	226(1)	525(1)
$\beta=4.35,\ a^{-1}=3.610(9),\ 48^3\times96\times8$	0.0120	0.0250	501(2)	620(2)
	0.0080	0.0250	408(2)	582(2)
	0.0042	0.0250	300(1)	547(2)
$\beta=4.47,\ a^{-1}=4.496(9),\ 64^3\times128\times8$	0.0030	0.0150	284(1)	486(1)

where $w = vv'$ is the recoil parameter defined by four velocities $v = p/M_B$ and $v' = p'/M_{D^{(*)}}$, and ε is a polarization vector of D^*, which satisfies $p'\varepsilon = 0$.

We employ the Möbius domain-wall action also for charm and bottom quarks to calculate $B \to D^*$ three-point functions. The charm quark mass m_c is set to its physical value determined from the spin averaged mass $(M_{\eta_c} + 3M_{J/\Psi})/4$, whereas we use the bottom masses $m_b = 1.25m_c, 1.25^2 m_c, \ldots$ under a condition $m_b < 0.7\,a^{-1}$ to suppress discretization effects. The $B \to D^{(*)}$ matrix elements can be extracted from the three-point functions, provided that they are dominated by their ground state contribution as

$$C^{BD^{(*)}}_{\mathscr{O}_\Gamma}(\Delta t, \Delta t'; \mathbf{p}, \mathbf{p}') \xrightarrow[\Delta t, \Delta t' \to \infty]{} \frac{Z^*_{D^{(*)}}(\mathbf{p}')\, Z_B(\mathbf{p})}{4E_{D^{(*)}}(\mathbf{p}')E_B(\mathbf{p})} \langle D^{(*)}(p')|\mathscr{O}_\Gamma|B(p)\rangle e^{-E_{D^{(*)}}(\mathbf{p}')\Delta t' - E_B(\mathbf{p})\Delta t}, \quad (2.4)$$

where $\mathscr{O}_\Gamma = V_\mu$ or A_μ, and the argument ε is suppressed for Z_{D^*} and $|D^*(p')\rangle$. We apply the Gaussian smearing to the interpolating field $\mathscr{O}_P$ ($P = B, D, D^*$) to enhance its overlap to the ground state $Z_P(\mathbf{p}) = \langle P(p)|\mathscr{O}_P^\dagger\rangle$. The B meson is at rest ($\mathbf{p} = \mathbf{0}$), and the w dependence of the form factors is studied by varying the three momentum of $D^{(*)}$ as $|\mathbf{p}'|^2 = 0, 1, 2, 3, 4$ in units of $(2\pi/L)^2$.

For precise determination of the form factors, we construct ratios of the correlation functions, in which unnecessary overlap factors and exponential damping factors cancel [20]. The statistical fluctuation is also expected to partly cancel. For instance, the normalizations, $h_+(1)$ and $h_{A_1}(1)$, and a ratio $R_1(w) = h_V(w)/h_{A_1}(w)$ can be directly extracted from the ratios

$$R^{BD^{(*)}}_{(k)}(\Delta t, \Delta t') = \frac{C^{BD^{(*)}}_{V_4(A_k)}(\Delta t, \Delta t'; \mathbf{0}, \mathbf{0})\, C^{D^{(*)}B}_{V_4(A_k)}(\Delta t, \Delta t'; \mathbf{0}, \mathbf{0})}{C^{BB}_{V_4(A_k)}(\Delta t, \Delta t'; \mathbf{0}, \mathbf{0})\, C^{D^{(*)}D^{(*)}}_{V_4(A_k)}(\Delta t, \Delta t'; \mathbf{0}, \mathbf{0})} \xrightarrow[\Delta t, \Delta t' \to \infty]{} |h_{+(A_1)}(1)|^2, \quad (2.5)$$

$$R^{BD^*}_{V,k}(\Delta t, \Delta t'; \mathbf{0}, \mathbf{p}'_\perp) = \frac{C^{BD^*}_{V_k}(\Delta t, \Delta t'; \mathbf{0}, \mathbf{p}'_\perp)}{C^{BD^*}_{A_k}(\Delta t, \Delta t'; \mathbf{0}, \mathbf{p}'_\perp)} \xrightarrow[\Delta t, \Delta t' \to \infty]{} \frac{\varepsilon_{ijk}\varepsilon^*_j v'_{\perp k}}{1+w} \frac{h_V(w)}{h_A(w)}, \quad (2.6)$$

where $\mathbf{p}'_\perp$ represents the D^* momentum satisfying $v\varepsilon = 0$. We refer the readers to Refs. [12, 21] for ratios to determine other form factors.

A salient feature of this analysis is that the form factors in Eqs. (2.1)–(2.3) can be calculated without finite renormalization of the local lattice operator $\mathscr{O}_\Gamma = V_\mu, A_\mu$ in Eq. (2.4). The relevant renormalization factors cancel in the correlator ratios with the relativistic heavy quarks with chiral symmetry. This is an advantage toward a precision calculation of the form factors, because we observe large discretization effects to the wave-function renormalization factor [13].

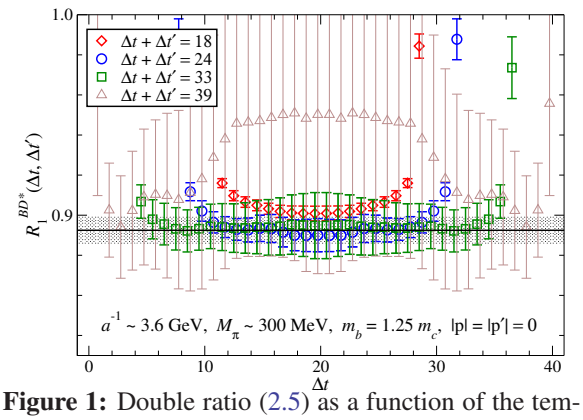

Figure 1: Double ratio (2.5) as a function of the temporal location Δt of A_μ. We plot data at $\beta = 4.35$, $m_{ud} = 0.0042$ and $m_b = 1.25\,m_c$. Symbols with different shapes show data with different values of $\Delta t + \Delta t'$. The shaded band shows a constant fit to estimate $|h_{A_1}(1)|^2$.

The choice of the source-sink separation $\Delta t + \Delta t'$ in Eq. (2.4) is also crucial for the precision study of heavy hadrons [22]. Except for the on-going simulation at the largest a^{-1} and smallest M_π, we repeat our measurement for four different values of $\Delta t + \Delta t'$ in a range 0.7 – 2.2 fm.

Figure 1, which shows the double ratio $R_1^{BD^*}(\Delta t, \Delta t')$, demonstrates that, towards larger separation, the three-point function has less excited state contamination, but its statistical noise rapidly grows. With the four values of $\Delta t + \Delta t'$, we can safely identify the plateau corresponding to the ground state dominance. The statistical accuracy is typically $1-2\%$ for h_+, h_{A_1} and h_V. Other form factors are less accurate, because i) h_- and h_{A_2} are close to zero due to heavy quark symmetry, and ii) we do not have matrix element, which is exclusively sensitive to h_{A_2} or h_{A_3}, partly due to our kinematical setup with the B meson at rest.

3. Continuum and chiral extrapolation

In this preliminary report, we extrapolate the form factors to the continuum limit and physical quark masses by using the following simple form based on the next-to-leading order (NLO) heavy meson chiral perturbation theory (HMChPT) [23, 24]

$$h_X = c + F_{\log}(M_\pi, f, \Lambda_\chi, g, \Delta_c) + c_w(w-1) + \frac{c_b}{m_b} + c_\pi M_\pi^2 + c_{\eta_s} M_{\eta_s}^2 + c_a a^2 + d_w(w-1)^2, \quad (3.1)$$

where $M_{\eta_s}^2 = 2M_K^2 - M_\pi^2 \sim 2m_s$ is used to describe the (presumably small) m_s dependence. The chiral log of, for instance, h_{A_1} is given as

$$F_{\log}(M_\pi, f, \Lambda_\chi, g, \Delta_c) = \frac{g^2}{32\pi^2 f^2} \bar{F}(M_\pi, \Delta_c, \Lambda_\chi). \quad (3.2)$$

We refer the readers to Refs. [23, 24] for the exact form of the loop integral function $\bar{F} = \Delta_c^2 \ln[M_\pi^2/\Lambda_\chi^2] + O(\Delta_c^3)$. The decay constant in the chiral limit f and the $D^* - D$ mass splitting Δ_c are fixed to the experimental value of the pion decay constant f_π and $M_{D^*} - M_D$, respectively. The renormalization scale of HMChPT is set to $\Lambda_\chi = 4\pi f_\pi$. These choices only modify the higher order chiral corrections. The coupling g is set to the value 0.53(8) quoted in Ref. [25], which covers the previous estimates of the $D^*D\pi$, $B^*B\pi$ couplings and their static limit. We note that, in this preliminary report, the quoted error is statistical only.

Figure 2 shows $B \to D^*\ell\nu$ form factors at simulated points and those extrapolated to the continuum limit and physical quark masses. Our result for $h_{A_1}(1)$ is in reasonable agreement with the previous estimate by Fermilab/MILC [25] and HPQCD [26]. We observe a mild dependence of the form factors on a^{-1} and quark masses, and the w dependence does not show any strong curvature in our simulation region near $w = 1$. As a result, many of fit parameters in Eq. (3.1) turned out to be consistent with zero. Only c, c_w and c_b for h_+, h_{A_1} and h_V have a statistical error less than 50 %. Since the parameter dependences are described reasonably well by a constant or linear term, this continuum and chiral extrapolation may not suffer from large systematic uncertainties, which are under investigation.

4. Implication to $|V_{cb}|$ determination

In the limit of $m_\ell = 0$, the $B \to D^*\ell\nu$ differential decay rate is described by $h_{A_1}(w)$ and two ratios $R_1(w)$ (defined above) and $R_2(w) = (rh_{A_2} + h_{A_3})/h_{A_1}$ ($r = M_{D^*}/M_B$) as

$$\frac{d\Gamma}{dw} \propto \frac{G_F^2 |V_{cb}|^2}{48\pi^3} \left[2\frac{1 - 2wr + r^2}{(1-r)^2} \left\{ 1 + \frac{w-1}{w+1} R_1(w)^2 \right\} + \left\{ 1 + \frac{w-1}{1-r}(1 - R_2(w)) \right\}^2 \right] h_{A_1}(w). \quad (4.1)$$

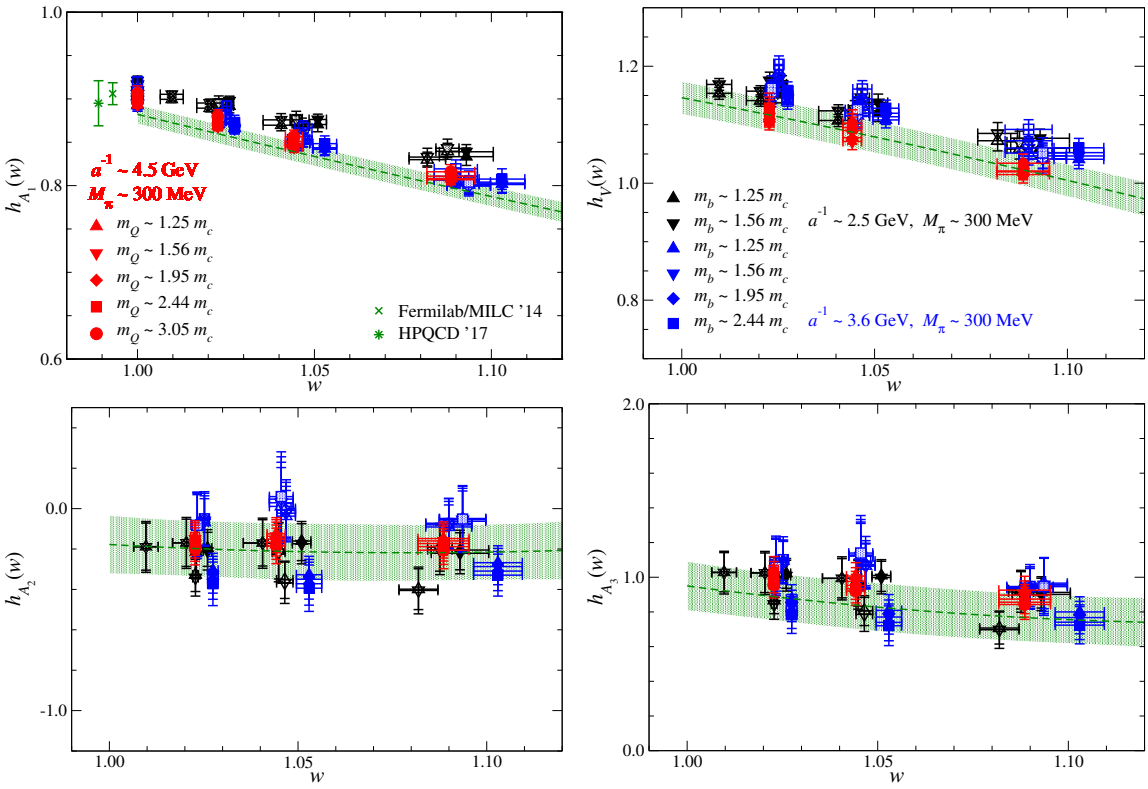

Figure 2: Form factors of the $B \to D^* \ell\nu$ decay as a function of w. Symbols show data at simulation points. Those extrapolated to the continuum limit and physical quark masses are plotted by the green bands. The red, blue, black symbols are obtained at $a^{-1} = 4.5$, 3.6 and 2.5 GeV, whereas open, pale shaded, filled, dark shaded symbols are at $M_\pi \sim 500$, 400, 300 and 230 MeV, respectively. Symbols with different shapes show data with different values of m_b. For $h_{A_1}(1)$, we also plot the previous estimates [25, 26].

The conventional determination of $|V_{cb}|$ employs the Caprini-Lellouch-Neubert (CLN) parametrization [27], in which h_{A_1}, R_1 and R_2 are expanded in terms of a small kinematical parameter and some of expansion coefficients are constrained by heavy quark effective theory (HQET) supplemented by the QCD sum rule inputs. Recent Belle data with the full kinematical distribution, on the other hand, enables an analysis with the Boyd-Grinstein-Lebed (BGL) parametrization without such HQET constraints and hence involving more free parameters.

It was reported a few years ago that i) model independent fit of the Belle tagged data [8] with the BGL parametrization yielded $|V_{cb}|$ consistent with the inclusive determination [3, 4], and that ii) there was a clear difference in R_1 between the BGL and CLN fits [6]. At last year's conference, we reported that our lattice data favor R_1 from the CLN fit. This is further confirmed by the additional data at the largest a^{-1} and smallest M_π as shown in the left panel of Fig. 3. Meanwhile, the BGL fit has been updated by including the Belle untagged data [9], and discrepancy from the CLN fit and lattice QCD has been resolved [7].

On the other hand, there has been no large difference in R_2 between the BGL and CLN fits as shown in the right panel of Fig. 3. Our lattice data are consistent with these phenomenological estimates within relatively large uncertainty coming from h_{A_2} and h_{A_3}. We note that this uncertainty is not problematic in predicting the differential decay rate (4.1), because the contribution of R_2 is suppressed by a factor $w-1$ in our simulation region near $w=1$. The left panel of Fig. 4

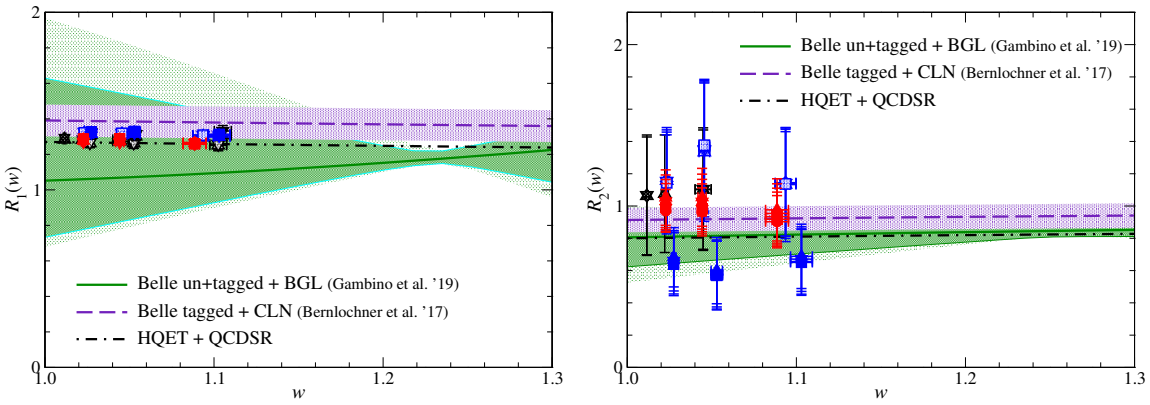

Figure 3: Form factor ratios R_1 (left panel) and R_2 (right panel) as a function of w. The symbols show our data at simulation points. The pale and dark shaded green bands show the results of the recent BGL fits with the standard and strong unitarity bounds [7], whereas the purple band is from the CLN fit [6]. We also plot the NLO HQET prediction by the dot-dashed line.

demonstrates that we can estimate $d\Gamma/dw$ with an accuracy comparable to experiments, and also shows a reasonable agreement between our and experimental data.

A ratio h_{A_1}/f_+, where f_+ is the vector form factor for $B \to D\ell\nu$, is also an important quantity, since the CLN parametrization of h_{A_1} is derived from this ratio in NLO HQET and a dispersive parametrization of f_+ [27]. The right panel of Fig. 4 shows a reasonable agreement in the w dependence between HQET and lattice QCD. While there is a ~ 10 % difference in the normalization, this does not necessarily lead to the $|V_{cb}|$ tension, since $h_{A_1}(1)$ is absorbed into the overall factor of $d\Gamma/dw$, which is treated as a fit parameter in the $|V_{cb}|$ determination.

5. Summary

In this article, we report on our studies of the $B \to D^{(*)}\ell\nu$ decays. The relevant form factors are precisely determined by simulating multiple values of the source-sink separation. While the systematics of the continuum and chiral extrapolation is under investigation, it is expected to be reasonably controllable due to the mild parametric dependence of the form factors.

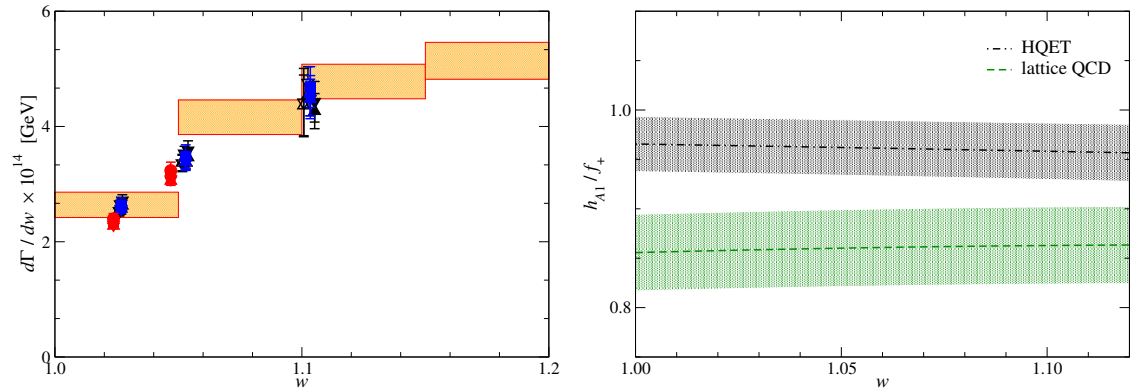

Figure 4: Left panel: $B \to D^*\ell\nu$ differential decay rate $d\Gamma/dw$ as a function of w. Symbols are estimated from our data at simulation points, whereas the orange band shows Belle data [8]. We assume $|V_{cb}|$ from $B \to D^*\ell\nu$ [1] to estimate $d\Gamma/dw$. Right panel: h_{A_1}/f_+ as a function of w. Our lattice result and the NLO HQET prediction are plotted by the green and black bands,respectively.

Recently, it is argued that the constraint in the CLN parametrization is responsible for the $|V_{cb}|$ tension. Except the normalization of h_{A_1}/f_+, our lattice data of h_{A_1}/f_+, R_1 and R_2 show a reasonable agreement with the CLN fit and NLO HQET. A more detailed analysis, such as the CLN and BGL fits both to lattice and experimental data, is needed towards an unambiguous resolution of the $|V_{cb}|$ tension.

We are grateful for F.U. Bernlochner, Z. Ligeti, M. Papucci, D.J. Robinson, and P. Gambino, M. Jung, S. Schacht for making their numerical results in Refs. [6, 7] available to us. Numerical simulations are performed on Oakforest-PACS at JCAHPC under a support of the HPCI System Research Projects (Project ID: hp180132 and hp190118) and Multidisciplinary Cooperative Research Program in CCS, University of Tsukuba (Project ID: xg18i016). This work is supported in part by JSPS KAKENHI Grant Number JP18H03710.

References

[1] Y. Amhis *et al.* (Heavy Flavor Averaging Group), Eur. Phys. J. C77 (2017) 895.
[2] F.U. Bernlochner, Z. Ligeti, M. Papucci, and D.J. Robinson, Phys. Rev. D 95 (2017) 115008.
[3] D. Bigi, P. Gambino and S. Schacht, Phys. Lett. B769 (2017) 441.
[4] B. Grinstein and A. Kobach, Phys. Lett. B771 (2017) 359.
[5] D. Bigi, P. Gambino and S. Schacht, JHEP 11 (2017) 061.
[6] F.U. Bernlochner, Z. Ligeti, M. Papucci and D.J. Robinson, Phys. Rev. D96 (2017) 091503.
[7] P. Gambino, M. Jung, S. Schacht, Phys. Lett. B795 (2019) 386
[8] A. Abdesselam *et al.* (Belle Collaboration), arXiv:1702.01521 [hep-ex].
[9] E. Waheed *et al.* (Belle Collaboration), Phys. Rev. D 100, 052007 (2019).
[10] A.V. Avilés-Casco *et al.* (Fermilab and MILC Collaboration), PoS (LATTICE2019) 049 in these proceedings.
[11] A. Lytle, PoS (LATTICE2019) 228 in these proceedings.
[12] T. Kaneko *et al.* (JLQCD Collaboration), PoS (LATTICE2018) 311.
[13] B. Fahy *et al.* (JLQCD Collaboration), PoS (LATTICE2016) 118.
[14] B. Colquhoun *et al.* (JLQCD Collaboration), PoS (LATTICE2018) 307.
[15] J. Koponen *et al.* (JLQCD Collaboration), PoS (LATTICE2019) 143 in these proceedings.
[16] G. Bailas *et al.* (JLQCD Collaboration), PoS (LATTICE2019) 148 in these proceedings.
[17] K. Nakayama and S. Hashimoto (JLQCD Collaboration), PoS (LATTICE2019) 062 in these proceedings.
[18] R.C. Brower, H. Neff and K. Orginos, Nucl. Phys. (Proc.Suppl.) 140 (2005) 686.
[19] T. Kaneko *et al.* (JLQCD Collaboration), PoS (LATTICE 2013) 125.
[20] S. Hashimoto *et al.*, Phys. Rev. D61 (1999) 014502.
[21] A.V. Avilés-Casco *et al.* (Fermilab and MILC Collaboration), EPJ Web Conf. 175 (2018) 13003.
[22] S. Hashimoto, PoS (LATTICE2018) 008.
[23] L. Randall and M.B. Wise, Phys. Lett. B303 (1993) 135.
[24] M.J. Savage, Phys. Rev. D65 (2002) 034014.
[25] J.A. Bailey *et al.* (Fermilab and MILC Collaboration), Phys. Rev. D 89 (2014) 114504.
[26] J. Harrison *et al.* (HPQCD Collaboration), Phys. Rev. D 97 (2018) 054502.
[27] I. Caprini, L. Lellouch, M. Neubert, Nucl. Phys. B530 (1998) 153.
[28] C.G. Boyd, B. Grinstein and R.F. Lebed, Phys. Rev. D56 (1997) 6895.